Monolayer $CrCl_3$ as an Ideal Test Bed for the Universality Classes of 2D Magnetism

M. Dupont,[1,2] Y. O. Kvashnin,[3] M. Shiranzaei,[3] J. Fransson,[3] N. Laflorencie,[4] and A. Kantian[5,3]
[1]Department of Physics, University of California, Berkeley, California 94720, USA
[2]Materials Sciences Division, Lawrence Berkeley National Laboratory, Berkeley, California 94720, USA
[3]Department of Physics and Astronomy, Uppsala University, Box 516, S-751 20 Uppsala, Sweden
[4]Laboratoire de Physique Théorique, IRSAMC, Université de Toulouse, CNRS, UPS, 31062 Toulouse, France
[5]SUPA, Institute of Photonics and Quantum Sciences, Heriot-Watt University, Edinburgh EH14 4AS, United Kingdom

(Received 13 January 2021; accepted 14 June 2021; published 16 July 2021)

The monolayer halides CrX_3 (X = Cl, Br, I) attract significant attention for realizing 2D magnets with genuine long-range order (LRO), challenging the Mermin-Wagner theorem. Here, we show that monolayer $CrCl_3$ has the unique benefit of exhibiting tunable magnetic anisotropy upon applying a compressive strain. This opens the possibility to use $CrCl_3$ for producing and studying both ferromagnetic and antiferromagnetic 2D Ising-type LRO as well as the Berezinskii-Kosterlitz-Thouless (BKT) regime of 2D magnetism with quasi-LRO. Using state-of-the-art density functional theory, we explain how realistic compressive strain could be used to tune the monolayer's magnetic properties so that it could exhibit any of these phases. Building on large-scale quantum Monte Carlo simulations, we compute the phase diagram of strained $CrCl_3$, as well as the magnon spectrum with spin-wave theory. Our results highlight the eminent suitability of monolayer $CrCl_3$ to achieve very high BKT transition temperatures, around 50 K, due to their singular dependence on the weak easy-plane anisotropy of the material.

DOI: 10.1103/PhysRevLett.127.037204

Introduction.—Two-dimensional (2D) systems are of unique importance to many-body quantum mechanics, as attested, e.g., by superconductivity in the cuprates [1] and at the LAO/STO interface [2], as well as graphene monolayers [3]. Part of this importance stems from the Mermin-Wagner (MW) theorem [4,5], which precludes any long-range order (LRO) arising from the spontaneous breaking of a continuous symmetry in two dimensions, but leaves room for a topological transition at finite temperature, named after Berezinskii [6], Kosterlitz, and Thouless [7,8] (BKT), e.g., in superfluid thin films [9] or 2D easy-plane (EP) magnets. Conversely, for easy-axis (EA) magnets, LRO due to the breaking of a discrete symmetry (e.g., $\mathbb{Z}_2$ for Ising systems) can occur at finite temperature. Such 2D magnets are at the forefront of both experiment and theory, not only for these fundamental reasons, but also for applications, ranging from spintronics [10,11] to both classical [12] and quantum information [11]. Based on the precise demands, materials in different universality classes of magnetic order may be desired, each of which may face specific fundamental challenges to be realized in two dimensions. Recently, genuine magnetic LRO has been observed in chromium halides CrX_3 (X = Cl, Br, I), which show local magnetic moments of spin greater than $1/2$, in the few—and monolayer regimes [13,14]. These results had substantial impact and induced much follow-up work in many other atomically thin van der Waals materials and their heterostructures [15,16].

First-principles density-functional theory (DFT) calculations show, and experiment confirms, that the insulating CrX_3 realizes highly localized magnetic moments close to $3\mu_B$ [17,18], corresponding to an ideal $S = 3/2$ system, with short-range, Heisenberg-like superexchange couplings, as well as local EA magnetic anisotropy. The latter allows CrX_3 to overcome the MW theorem and to establish 2D magnetic LRO [19,20]. These traits imbue CrX_3 with a major advantage compared to gapless itinerant magnets [21]. It is then $CrCl_3$ specifically that has unique potential for realizing magnetic universality classes beyond those with LRO, as it shows only a small EA anisotropy due to its lighter ligand, making it the most amenable to sign change by external manipulation, and thus realizing an EP anisotropy instead [17]. DFT study further predicts that the anisotropy of the exchange in $CrCl_3$ is sufficiently suppressed [22]. In contrast, bulk and monolayers of $CrBr_3$ and CrI_3 are predicted to show strong EA anisotropy (both single-ion and intersite) for which achieving sign change would be unrealistic. This strong anisotropy arises from the spin-orbit coupling emerging from the heavier ligands [23,24], and CrI_3 further also displays strongly anisotropic exchange (possibly stemming from Kitaev interactions) [25,26].

Thus the opportunity to turn EA into EP anisotropy in $CrCl_3$ via compressive strain raises the possibility of tuning a material across strikingly different universality classes, with remarkable critical properties. Of greatest interest in this respect is the BKT regime, marked by the appearance of topological vortex excitations. Below a critical temperature the BKT regime exhibits quasi-LRO, i.e., with critical algebraic correlations. But while the realization of the

quasi-LRO regime was first proposed for magnetic systems [7], it has been surprisingly difficult to detect in such. In the various layered bulk magnets in which it is sought at low temperatures, there is invariably a temperature scale below which the weak coupling between the 2D layers gives rise to an effective 3D regime [27,28] with its attendant magnetic LRO, obscuring the sought-after BKT physics [29,30].

In this Letter, we propose that, among the monolayer halides, $CrCl_3$ provides unique advantages for tuning material properties using, e.g., externally applied pressure such that both 2D Ising ferromagnetic (FM) and antiferromagnetic (AFM) states with LRO as well as the sought-after BKT universality class could be observed, all in the same material. This ability is based on monolayer $CrCl_3$ realizing a 2D spin-3/2 Heisenberg-like Hamiltonian with local anisotropy on a honeycomb lattice with high fidelity, where both nearest-neighbor superexchange coupling and magnetic anisotropy are susceptible to tuning of both their magnitude and sign due to strain ε caused by realistic external pressure. Most pertinently, this in turn yields a BKT transition that is predicted to occur at much higher temperatures than true LRO in the layered bulk material [31], found to be around 17 K at zero strain [32], see Fig. 1(d). We further calculate the spin-excitation spectra of the material in the various strain regimes using the spin-wave approximation.

DFT of the monolayer and the effect of strain.—The general crystal structure of monolayer $CrCl_3$ is depicted in Fig. 1(a). Within our DFT approach, we first obtain the equilibrium structure of the crystal. Then, we strain the lattice while allowing Cl atoms to adjust their positions in order to minimize the energy cost of the lattice deformation at each chosen value of strain ε. For every structure generated, we compute the total energy difference between FM and AFM states. This allows us to extract the effective value of the nearest-neighbour exchange coupling J_ε by mapping the energy difference onto Hamiltonian:

$$\hat{H} = J_\varepsilon \sum_{\langle \boldsymbol{r},\boldsymbol{r}'\rangle} \hat{\boldsymbol{S}}_{\boldsymbol{r}} \cdot \hat{\boldsymbol{S}}_{\boldsymbol{r}'} + K_\varepsilon \sum_{\boldsymbol{r}} (\hat{S}^z_{\boldsymbol{r}})^2, \tag{1}$$

where $\hat{\boldsymbol{S}}_{\boldsymbol{r}} = (\hat{S}^x_{\boldsymbol{r}}, \hat{S}^y_{\boldsymbol{r}}, \hat{S}^z_{\boldsymbol{r}})$ are the standard $S = 3/2$ spin-operators positioned on the vertices of a 2D honeycomb lattice. The sum $\langle \boldsymbol{r}, \boldsymbol{r}'\rangle$ restricts the magnetic exchange to nearest-neighbor spins. We perform fully relativistic calculations in order to compute the magnetic anisotropy K_ε, calculating the total energy difference between in-plane and out-of-plane orientations of the magnetization; for details, see the Supplemental Material [33]. Our approach is in line with previous work studying the magnetic properties of CrX_3 [23,25,51–56], which we note to yield critical temperatures in excellent agreement with experiment (see, e.g., Ref. [32]). Our own DFT treatment results in a nearest-neighbour distance for the Cr atoms of 3.424 Å at $\varepsilon = 0\%$, thus matching the measured bulk value of 3.44 Å [57,58], signifying the accuracy of our approach.

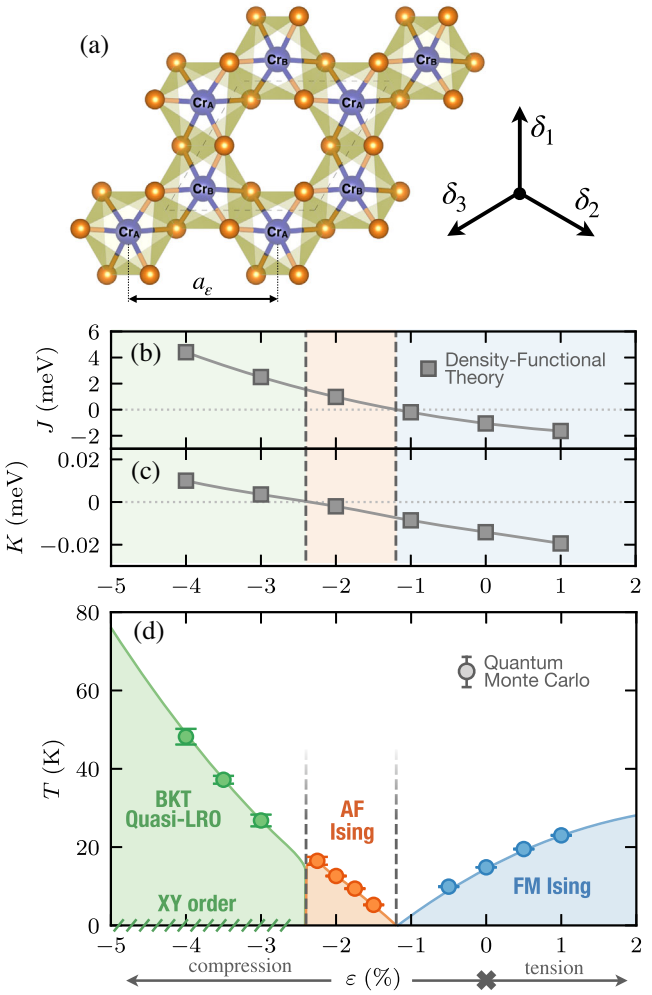

FIG. 1. (a) Crystal structure of monolayer $CrCl_3$. The Cr and Cl atoms are represented in blue and orange, respectively. The $\mathcal{A}$ and $\mathcal{B}$ sublattices of Cr is indicated. Dashed lines denote the unit cell with basic vectors $\boldsymbol{\delta}_1 = a_\varepsilon(0,1)$, $\boldsymbol{\delta}_2 = a_\varepsilon(\sqrt{3}/2, -1/2)$, $\boldsymbol{\delta}_3 = a_\varepsilon(-\sqrt{3}/2, -1/2)$, with strain-dependent lattice constant a_ε. (b)–(c) Magnetic nearest-neighbor superexchange J and anisotropy K of Hamiltonian (1), respectively, computed via DFT as a function of monolayer strain ε. (d) Finite-temperature phase diagram of the monolayer $CrCl_3$ versus strain ε, obtained by QMC simulations for the $S = 3/2$ model of Eq. (1) on the 2D honeycomb lattice. Strain drives the monolayer into three different finite-temperature magnetic phases: BKT quasi-LRO phase for $\varepsilon \lesssim -2.4\%$, AFM Ising for $-2.4\% \lesssim \varepsilon \lesssim -1.2\%$, and FM Ising for $\varepsilon \gtrsim -1.2\%$. At zero temperature, the BKT quasi-LRO turns into genuine XY LRO, separated from the AFM Ising order by an isotropic Heisenberg point displaying Néel order (where K_ε vanishes). The AFM and FM Ising phases are separated by a trivial paramagnetic point (where J_ε vanishes). The colored lines are fits to the form of Eq. (2).

We present our results for the Hamiltonian parameters J_ε and K_ε as a function of material strain ε in Figs. 1(b) and 1(c). It shows the FM configuration to be energetically

favored at zero strain, in line with bulk $CrCl_3$, and the magnetic anisotropy to be of EA type and pointing out of plane, opposite to what is known for the bulk [17]. This change in the monolayer limit has been obtained in prior DFT-based studies however [51,59–61]. As compressive strain is applied to the monolayer, two key features of Figs. 1(b) and 1(c) stand out: the sign change of J_ε at $\varepsilon = -1.2\%$ from FM at AFM coupling, and of K_ε at $\varepsilon = -2.4\%$ from EA to EP anisotropy as strain increases. These results validate our initial hypothesis that the much weaker magnetic anisotropy of monolayer $CrCl_3$ compared to CrI_3 and $CrBr_3$ offers an ideal platform to modify the Hamiltonian symmetry and thus explore Ising-type 2D magnetism of both the FM and AFM variant (for $K_\varepsilon < 0$), as well as the BKT regime (for $K_\varepsilon > 0$), as the strains necessary are readily available in the lab; a strain of, e.g., -4% corresponds to pressure of 0.7 GPa.

While a different choice of DFT exchange-correlation functional predicts a different K_ε [51], we note that our own choice, also used in, e.g., Ref. [22], yields a better match to the experimentally found lattice constant, Cr-Cl distance and Cr-Cl-Cr bond angle at $\varepsilon = 0\%$, as well as yielding qualitatively the same phase diagram [33].

Our analysis reveals the source of the sign change in J_ε as a subtle shift in balance between competing FM and AFM contributions, which we explicitly show in the Supplemental Material [33]. According to the theory of superexchange [19,20,34], there is a FM superexchange between half-filled t_{2g} and nominally empty e_g orbital on the neighboring Cr atoms, mediated by a single Cl-3p orbital [22,35,36]. This contribution is opposed by AFM superexchange between two different t_{2g} orbitals via Cl state and also by the direct kinetic AFM exchange between the t_{2g} orbitals pointing towards each other. Compressive strain on the monolayer decreases the Cr-Cr distance and increases the orbital overlap. While it is hard to say how superexchange paths are affected, the latter is definitely expected to boost the AFM kinetic exchange term, which we argue to be the main driving force for the change of sign of J_ε upon compressive strain.

From Ising to BKT.—Building on the DFT-calculated couplings J_ε and K_ε, we perform large-scale QMC simulations of the $S = 3/2$ Hamiltonian of Eq. (1) [33]. We simulate 2D systems of $N = 2 \times L \times L$ spins on the honeycomb lattice, up to $N \approx 5 \times 10^4$, and map the phase diagram as a function of the strain ε for $CrCl_3$, as shown in Fig. 1(d).

For $K_\varepsilon < 0$ ($\varepsilon > -2.4\%$) in the EA regime, we perform a finite-size scaling analysis of the magnetic order parameter in order to extract the critical temperature T_c for the onset of magnetic LRO, perfectly supporting the 2D Ising universality class. This is exemplified in Figs. 2(a) and 2(b) where we find the thermal melting of both FM order for $\varepsilon > -1.2\%$, and AFM order for $\varepsilon \in [-2.4\%, -1.2\%]$, to be precisely described by the critical exponents $\beta = 1/8$ for the order parameter, and $\nu = 1$ for the correlation length [37], allowing for accurate extraction of T_c.

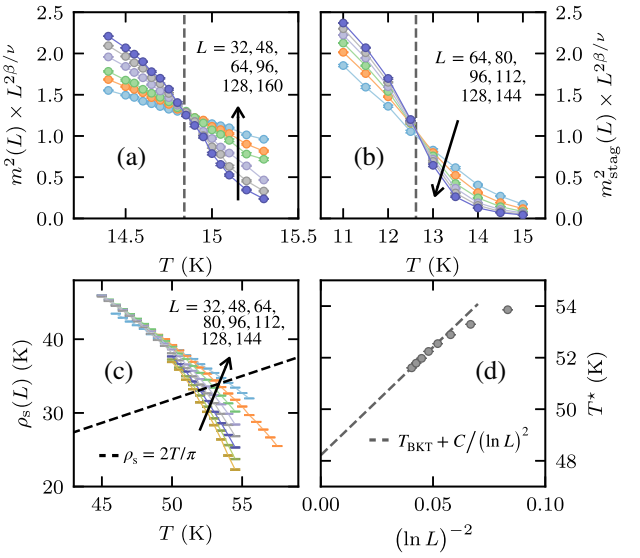

FIG. 2. (a)–(b) Obtaining T_c (dashed vertical lines) for onset of magnetic LRO from scaling analysis of QMC values of the order parameter in the EA regime, using 2D Ising critical exponents $\beta = 1/8$ and $\nu = 1$. (a) Magnetization density vs temperature for different L at $\varepsilon = 0\%$ (FM Ising), with $T_c = 14.84(1)$ K. (b) Staggered magnetization density vs temperature for different L at $\varepsilon = -2\%$ (AFM Ising), with $T_c = 12.6(1)$ K. (c) Finite-size scaling analysis of QMC-computed spin stiffness $\rho_s(L)$ at different L in EA regime, at $\varepsilon = -4\%$ (BKT Quasi-LRO). Dashed line shows $2T/\pi$. (d) $T^\star(L)$ extracted from (c) vs $(\ln L)^{-2}$ for $\varepsilon = -4\%$. $T_{\mathrm{BKT}} = 48(2)$ K is extracted from fitting with $T_{\mathrm{BKT}} + C/(\ln L)^2$ (dashed line).

When entering the EP regime for $K_\varepsilon > 0$ ($\varepsilon < -2.4\%$), there is a drastic change in the critical properties. At zero temperature, true LRO is expected, breaking the U(1) symmetry, but at finite temperature the MW theorem precludes this [4,5], allowing at most for quasi-LRO in the XY plane. This is what we observe for $\varepsilon = -4\%$ in Fig. 2(c), where the system displays a finite spin stiffness $\rho_s(T)$ below a transition temperature $T_{\mathrm{BKT}} \sim 50$ K. Another manifestation of the transition to quasi-LRO is the onset of algebraic decay of spin correlations [33]. We determine T_{BKT} both from the universal relation $\rho_s(T = T_{\mathrm{BKT}}) = 2T_{\mathrm{BKT}}/\pi$ [62], see Fig. 2(c), as well as from critical correlations decaying with a universal exponent $\eta = 1/4$ [8,33]. Yet, strong logarithmic finite-size corrections are expected for BKT transitions [8,63,64], calling for a careful analysis. Noting $T^\star(L)$ the solution of $\rho_s(L) = 2\pi/T$, we extract the thermodynamic limit estimate of T_{BKT} through the relation [65] $T^\star(L) = T_{\mathrm{BKT}} + C/(\ln L)^2$, valid as $L \to +\infty$, with C a nonuniversal constant, as exemplified in Fig. 2(d) for $\varepsilon = -4\%$, where we obtain $T_{\mathrm{BKT}} = 48(2)$ K. Several estimates are reported in Fig. 1(d), where we observe a strong enhancement of T_{BKT} upon compressive strain for $\varepsilon < -2.4\%$. This

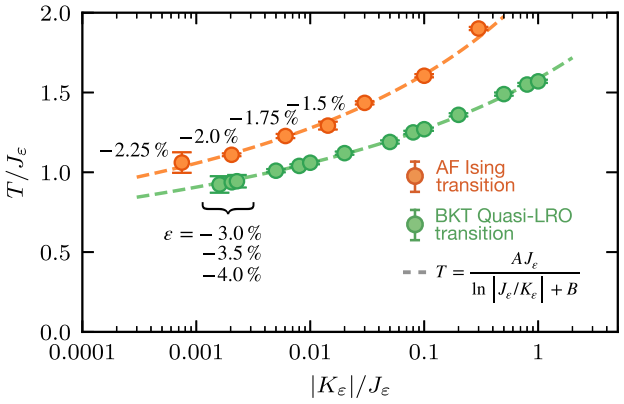

FIG. 3. Critical temperature T_c (AFM Ising, orange) and T_{BKT} (BKT Quasi-LRO, green) vs $|K_\varepsilon|/J_\varepsilon$. Points with explicit ε values correspond to $K_\varepsilon/J_\varepsilon$ for monolayer $CrCl_3$ at such strain, see Fig. 1(d). Dashed lines show fit to $A/(\ln|J_\varepsilon/K_\varepsilon| + B)$ in the small anisotropy limit $|K_\varepsilon|/J_\varepsilon \leq 0.1$, with A and B fitting parameters. For BKT, $A = 14.6(3)$, $B = 9.2(3)$. For AFM Ising, $A = 14.1(5)$, $B = 6.5(4)$. Both A values are compatible with the analytical prediction $A = 4\pi\rho_s^{(0)} = 16(1)$ in Eq. (2).

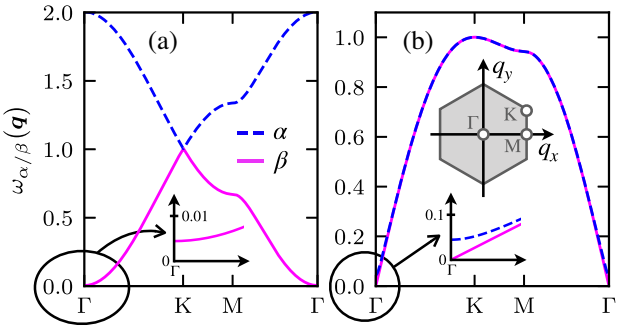

FIG. 4. Band structure of magnons in (a) easy-axis FM and (b) easy-plane AFM. The blue and magenta curves represent α and β bands, respectively. Inset in panel (a) shows gap opening at the bottom of spectrum close to Γ due to anisotropy while the one in panel (b) displays breaking of band degeneracy close to Γ. The Brillouin zone of the honeycomb lattice is displayed in (b), along with the high symmetry points $\boldsymbol{q} = a_\varepsilon^{-1}(q_x, q_y)$: $\Gamma = a_\varepsilon^{-1}(0,0)$, $M = a_\varepsilon^{-1}(4\pi/3, 0)$, and $K = a_\varepsilon^{-1}(\pi, \pi/\sqrt{3})$ with strain-dependent lattice constant a_ε.

remarkable increase is not directly controlled by the $SU(2) \to U(1)$ symmetry breaking term K_ε in the Hamiltonian Eq. (1), but emerges from a strong non-linear effect, as we discuss now.

Logarithmic enhancement of the critical temperature.—The critical nature of 2D systems at low temperatures results in a strong sensitivity to even weak anisotropies ($|K_\varepsilon/J_\varepsilon|$ is typically less than $\approx 10^{-2}$) that nudge the system towards a certain (quasi-)order. Thus, in line with previous work on alternative realizations of 2D magnets [66–68], we find a strong logarithmic enhancement of critical temperatures, which are controlled by the exchange J_ε but also with a singular dependence on K_ε, both on the Ising and on the BKT side for the $CrCl_3$ monolayer, as clearly shown in Fig. 3. Using QMC for both physical parameters at various strains, as well as a broader range for the ratio $|K_\varepsilon|/J_\varepsilon$, we find excellent agreement with

$$T_{c,\mathrm{BKT}} = \frac{4\pi J_\varepsilon \rho_s^{(0)}}{\ln|J_\varepsilon/K_\varepsilon| + B}, \tag{2}$$

where $\rho_s^{(0)}$ is the dimensionless spin stiffness of the isotropic ($K_\varepsilon = 0$) system at zero temperature and B is a nonuniversal constant [67,68]. A QMC estimate of the isotropic stiffness gives a prefactor $4\pi\rho_s^{(0)} = 16(1)$, which agrees well with our results displayed in Fig. 3.

Magnon-spectra of the monolayer.—Complementing our QMC description of the equilibrium properties we use spin-wave (SW) analysis for an N-site cluster of the system Hamiltonian (1) to obtain predictions for the $T = 0$ excitation spectrums of the monolayer at $\varepsilon = 0\%$ (FM phase) and $\varepsilon = -4\%$ (XY order), see Fig. 1(d). In each case we model the deviations of the spins around a classical configuration, with the analytical procedure depending on whether this configuration is externally proscribed or has to be picked randomly.

For $K_\varepsilon < 0$ ($\varepsilon = 0\%$), the ground-state configuration is of the spins aligned out of plane in the z direction. We use the appropriate Holstein-Primakoff (HP) transformation [38] for mapping the magnon excitations above the ground state onto noninteracting bosons [33]. Up to quadratic terms and after canonical transformations, one arrives at

$$\frac{\hat{H}}{NS^2} \approx -\frac{3J_\varepsilon}{2} - K_\varepsilon + \frac{3J_\varepsilon}{NS}\sum_{\boldsymbol{q}}[\omega_\alpha(\boldsymbol{q})\hat{\alpha}_{\boldsymbol{q}}^\dagger\hat{\alpha}_{\boldsymbol{q}} + \omega_\beta(\boldsymbol{q})\hat{\beta}_{\boldsymbol{q}}^\dagger\hat{\beta}_{\boldsymbol{q}}], \tag{3}$$

for approximating the magnon spectrum as the dispersion of two distinct types of free bosons, with

$$\omega_{\alpha/\beta}(\boldsymbol{q}) = 1 + \frac{K_\varepsilon}{3J_\varepsilon} \pm |\gamma(\boldsymbol{q})|, \tag{4}$$

where $\gamma(\boldsymbol{q}) = (1/3)\sum_{n=1}^{3} e^{i\boldsymbol{q}\cdot\boldsymbol{\delta}_n}$ and $\boldsymbol{\delta}_n$-vectors as shown in Fig. 1(a). The EA anisotropy is seen to open a gap at the bottom of the lower β branch, which stabilizes the system against the long-wavelength Goldstone modes that would otherwise result in the destruction of magnetic LRO, see Fig 4(a).

For $K_\varepsilon > 0$ ($\varepsilon = -4\%$), when the anisotropy becomes EP due to compressive strain, one has to pick an arbitrary orientation in the XY plane along which the spins order; we chose the x direction in the following. For the concrete $CrCl_3$ monolayer this procedure is justified by our DFT results, which show energy differences for different in-plane orientations to be well below the μeV level. Application of the standard HP-approach would violate

the Goldstone theorem, so we use the matching of matrix-elements (MME) technique instead [33,39,40]. As spin-exchange dominates, we expand to the first power of $d_\varepsilon = K_\varepsilon/6J_\varepsilon S$. This results in another magnon-Hamiltonian structurally analogous to the one presented in Eq. (3), but with the ground state energy replaced by $NS\{-3J_\varepsilon S + K_\varepsilon[1 - d_\varepsilon(2S-1)]\}/2$ and the dispersion relation

$$\omega_{\alpha/\beta}(\boldsymbol{q}) = \sqrt{\{1 + d_\varepsilon(2S-1)[1 \pm |\gamma(\boldsymbol{q})|]\}^2 - |\gamma(\boldsymbol{q})|^2}. \tag{5}$$

As shown in Fig. 4(b), the magnon spectrum now is mostly degenerate except around the $\boldsymbol{\Gamma}$ point where the EP anisotropy breaks the degeneracy, gapping the α branch while the β branch remains linear down to $\boldsymbol{q} = \boldsymbol{0}$, thus signaling the presence of a Nambu-Goldstone mode associated with the breaking of the U(1) symmetry.

Discussion and outlook.—Various signatures would be available in order to detect the transition of monolayer $CrCl_3$ to the BKT regime that we have shown to happen as compressive strain is increased. The decay-behavior of an induced spin-current as, e.g., emanating from a Pt electrode has been proposed for this [69]. So has been the minimum in the uniform magnetic zz susceptibility predicted to occur for 2D EP magnets just above the BKT transition, as opposed to the monotonous decline predicted for the xx susceptibility [70]. In that respect, the 2D honeycomb $S = 1$ AFM compound $BaNi_2V_2O_8$ [71,72] was very recently shown to be a good candidate [73]. These susceptibilities are practically accessible in current experiments on compressed monolayers. Crucially, the monolayer of $CrCl_3$ would not suffer from some intervening onset of 3D magnetism which has obscured experimental studies of the BKT regime in layered bulk magnets thus far. The sum of the present work shows this material to be ideally situated in parameter space in order to address the major universality classes of 2D magnetism with great control and accuracy.

A. K. would like to thank M. Abdel-Hafiez for fruitful discussions. M. D. was supported by the U.S. Department of Energy, Office of Science, Office of Basic Energy Sciences, Materials Sciences and Engineering Division under Contract No. DE-AC02-05-CH11231 through the Scientific Discovery through Advanced Computing (SciDAC) program (KC23DAC Topological and Correlated Matter via Tensor Networks and Quantum Monte Carlo). Y. O. K. (Project No. 2019-03569) and J. F. acknowledge financial support from Swedish Research Council (VR). M. Sh. and J. F. thank Carl Tryggers Stiftelse for financial support. N. L. acknowledges the French National Research Agency (ANR) under Projects THERMOLOC ANR-16-CE30-0023-02, and GLADYS ANR-19-CE30-0013. This research used the Lawrencium computational cluster resource provided by the IT Division at the Lawrence Berkeley National Laboratory (Supported by the Director, Office of Science, Office of Basic Energy Sciences, of the U.S. Department of Energy under Contract No. DE-AC02-05CH11231). This research also used resources of the National Energy Research Scientific Computing Center (NERSC), a U.S. Department of Energy Office of Science User Facility operated under Contract No. DE-AC02-05CH11231. The DFT computations were performed using the resources provided by the Swedish National Infrastructure for Computing (SNIC) at the National Supercomputing Centre (NSC).

[1] B. Keimer, S. A. Kivelson, M. R. Norman, S. Uchida, and J. Zaanen, Nature (London) **518**, 179 (2015).
[2] N. Reyren, S. Thiel, A. D. Caviglia, L. F. Kourkoutis, G. Hammerl, C. Richter, C. W. Schneider, T. Kopp, A.-S. Rüetschi, D. Jaccard, M. Gabay, D. A. Muller, J.-M. Triscone, and J. Mannhart, Science **317**, 1196 (2007).
[3] K. S. Novoselov, A. K. Geim, S. V. Morozov, D. Jiang, M. I. Katsnelson, I. V. Grigorieva, S. V. Dubonos, and A. A. Firsov, Nature (London) **438**, 197 (2005).
[4] N. D. Mermin and H. Wagner, Phys. Rev. Lett. **17**, 1133 (1966).
[5] P. C. Hohenberg, Phys. Rev. **158**, 383 (1967).
[6] V. Berezinsky, Sov. Phys. JETP **32**, 493 (1971), http://www.jetp.ac.ru/cgi-bin/e/index/e/32/3/p493?a=list.
[7] J. M. Kosterlitz and D. J. Thouless, J. Phys. C **6**, 1181 (1973).
[8] J. M. Kosterlitz, J. Phys. C **7**, 1046 (1974).
[9] D. J. Bishop and J. D. Reppy, Phys. Rev. Lett. **40**, 1727 (1978).
[10] L. N. Kapoor, S. Mandal, P. C. Adak, M. Patankar, S. Manni, A. Thamizhavel, and M. M. Deshmukh, Adv. Mater. **33**, 2005105 (2021).
[11] V. P. Ningrum, B. Liu, W. Wang, Y. Yin, Y. Cao, C. Zha, H. Xie, X. Jiang, Y. Sun, S. Qin, X. Chen, T. Qin, C. Zhu, L. Wang, and W. Huang, Research **2020**, 1 (2020).
[12] T. Song, X. Cai, M. W.-Y. Tu, X. Zhang, B. Huang, N. P. Wilson, K. L. Seyler, L. Zhu, T. Taniguchi, K. Watanabe, M. A. McGuire, D. H. Cobden, D. Xiao, W. Yao, and X. Xu, Science **360**, 1214 (2018).
[13] C. Gong, L. Li, Z. Li, H. Ji, A. Stern, Y. Xia, T. Cao, W. Bao, C. Wang, Y. Wang, Z. Q. Qiu, R. J. Cava, S. G. Louie, J. Xia, and X. Zhang, Nature (London) **546**, 265 (2017).
[14] B. Huang, G. Clark, E. Navarro-Moratalla, D. R. Klein, R. Cheng, K. L. Seyler, D. Zhong, E. Schmidgall, M. A. McGuire, D. H. Cobden, W. Yao, D. Xiao, P. Jarillo-Herrero, and X. Xu, Nature (London) **546**, 270 (2017).
[15] K. S. Burch, D. Mandrus, and J.-G. Park, Nature (London) **563**, 47 (2018).
[16] M. Gibertini, M. Koperski, A. F. Morpurgo, and K. S. Novoselov, Nat. Nanotechnol. **14**, 408 (2019).
[17] M. A. McGuire, G. Clark, S. KC, W. M. Chance, G. E. Jellison, V. R. Cooper, X. Xu, and B. C. Sales, Phys. Rev. Mater. **1**, 014001 (2017).
[18] J. F. Dillon and C. E. Olson, J. Appl. Phys. **36**, 1259 (1965).

[19] P. W. Anderson, Phys. Rev. **115**, 2 (1959).
[20] J. Kanamori, J. Phys. Chem. Solids **10**, 87 (1959).
[21] A. O. Fumega, M. Gobbi, P. Dreher, W. Wan, C. González-Orellana, M. Peña-Díaz, C. Rogero, J. Herrero-Martín, P. Gargiani, M. Ilyn, M. M. Ugeda, V. Pardo, and S. Blanco-Canosa, J. Phys. Chem. C **123**, 27802 (2019).
[22] Y. O. Kvashnin, A. Bergman, A. I. Lichtenstein, and M. I. Katsnelson, Phys. Rev. B **102**, 115162 (2020).
[23] J. L. Lado and J. Fernández-Rossier, 2D Mater. **4**, 035002 (2017).
[24] T. A. Tartaglia, J. N. Tang, J. L. Lado, F. Bahrami, M. Abramchuk, G. T. McCandless, M. C. Doyle, K. S. Burch, Y. Ran, J. Y. Chan, and F. Tafti, Sci. Adv. **6**, eabb9379 (2020).
[25] C. Xu, J. Feng, H. Xiang, and L. Bellaiche, npj Comput. Mater. **4**, 57 (2018).
[26] I. Lee, F. G. Utermohlen, D. Weber, K. Hwang, C. Zhang, J. van Tol, J. E. Goldberger, N. Trivedi, and P. C. Hammel, Phys. Rev. Lett. **124**, 017201 (2020).
[27] S. C. Furuya, M. Dupont, S. Capponi, N. Laflorencie, and T. Giamarchi, Phys. Rev. B **94**, 144403 (2016).
[28] S. Allenspach, A. Biffin, U. Stuhr, G. S. Tucker, S. Ohira-Kawamura, M. Kofu, D. J. Voneshen, M. Boehm, B. Normand, N. Laflorencie, F. Mila, and C. Rüegg, Phys. Rev. Lett. **124**, 177205 (2020).
[29] U. Tutsch, B. Wolf, S. Wessel, L. Postulka, Y. Tsui, H. O. Jeschke, I. Opahle, T. Saha-Dasgupta, R. Valentí, A. Brühl, K. Remović-Langer, T. Kretz, H. W. Lerner, M. Wagner, and M. Lang, Nat. Commun. **5**, 5169 (2014).
[30] Z. Hu, Z. Ma, Y.-D. Liao, H. Li, C. Ma, Y. Cui, Y. Shangguan, Z. Huang, Y. Qi, W. Li, Z. Y. Meng, J. Wen, and W. Yu, Nat. Commun. **11**, 5631 (2020).
[31] J. Cable, M. Wilkinson, and E. Wollan, J. Phys. Chem. Solids **19**, 29 (1961).
[32] D. Soriano, M. I. Katsnelson, and J. Fernández-Rossier, Nano Lett. **20**, 6225 (2020).
[33] See Supplemental Material at http://link.aps.org/supplemental/10.1103/PhysRevLett.127.037204 for technical information regarding the DFT calculations, the QMC simulations, and the spin-wave analysis. We also provide details regarding the finite-size scaling analyses of the QMC data for the FM Ising, AFM Ising, and BKT regimes. Finally, we provide a discussion on the different exchange paths in $CrCl_3$ and additional DFT results using the PBE functional. See also Refs. [19,34–51] therein.
[34] J. B. Goodenough, J. Phys. Chem. Solids **6**, 287 (1958).
[35] O. Besbes, S. Nikolaev, N. Meskini, and I. Solovyev, Phys. Rev. B **99**, 104432 (2019).
[36] I. V. Kashin, V. V. Mazurenko, M. I. Katsnelson, and A. N. Rudenko, 2D Mater. **7**, 025036 (2020).
[37] J. Cardy, P. Goddard, and J. Yeomans, *Scaling and Renormalization in Statistical Physics*, Cambridge Lecture Notes in Physics (Cambridge University Press, Cambridge, England, 1996).
[38] T. Holstein and H. Primakoff, Phys. Rev. **58**, 1098 (1940).
[39] P. A. Lindgard and A. Kowalska, J. Phys. C **9**, 2081 (1976).
[40] U. Balucani, M. G. Pini, and V. Tognetti, J. Phys. C **13**, 2925 (1980).
[41] G. Kresse and D. Joubert, Phys. Rev. B **59**, 1758 (1999).
[42] G. Kresse and J. Furthmüller, Comput. Mater. Sci. **6**, 15 (1996).
[43] J. P. Perdew, A. Ruzsinszky, G. I. Csonka, O. A. Vydrov, G. E. Scuseria, L. A. Constantin, X. Zhou, and K. Burke, Phys. Rev. Lett. **100**, 136406 (2008).
[44] O. F. Syljuåsen and A. W. Sandvik, Phys. Rev. E **66**, 046701 (2002).
[45] F. Alet, S. Wessel, and M. Troyer, Phys. Rev. E **71**, 036706 (2005).
[46] B. Bauer *et al.*, J. Stat. Mech. 05 (2011) P05001.
[47] A. Dorneich and M. Troyer, Phys. Rev. E **64**, 066701 (2001).
[48] E. L. Pollock and D. M. Ceperley, Phys. Rev. B **36**, 8343 (1987).
[49] A. W. Sandvik, Phys. Rev. B **56**, 11678 (1997).
[50] J. P. Perdew, K. Burke, and M. Ernzerhof, Phys. Rev. Lett. **77**, 3865 (1996).
[51] L. Webster and J.-A. Yan, Phys. Rev. B **98**, 144411 (2018).
[52] J. Liu, Q. Sun, Y. Kawazoe, and P. Jena, Phys. Chem. Chem. Phys. **18**, 8777 (2016).
[53] X. Lu, R. Fei, and L. Yang, Phys. Rev. B **100**, 205409 (2019).
[54] C. Xu, J. Feng, S. Prokhorenko, Y. Nahas, H. Xiang, and L. Bellaiche, Phys. Rev. B **101**, 060404(R) (2020).
[55] T. Olsen, MRS Commun. **9**, 1142 (2019).
[56] M. Pizzochero, R. Yadav, and O. V. Yazyev, 2D Mater. **7**, 035005 (2020).
[57] B. Morosin and A. Narath, J. Chem. Phys. **40**, 1958 (1964).
[58] M. A. McGuire, Crystals **7**, 121 (2017).
[59] W.-B. Zhang, Q. Qu, P. Zhu, and C.-H. Lam, J. Mater. Chem. C **3**, 12457 (2015).
[60] F. Xue, Y. Hou, Z. Wang, and R. Wu, Phys. Rev. B **100**, 224429 (2019).
[61] Reference [60] suggests that the magnetic shape anisotropy in the unstrained monolayer $CrCl_3$ could overcome the magnetocrystalline anisotropy. We have not considered this effect, which would be problematic to treat in QMC.
[62] D. R. Nelson and J. M. Kosterlitz, Phys. Rev. Lett. **39**, 1201 (1977).
[63] N. Laflorencie, S. Capponi, and E. S. Sørensen, Eur. Phys. J. Spec. Top. **24**, 77 (2001).
[64] Y.-D. Hsieh, Y.-J. Kao, and A. W. Sandvik, J. Stat. Mech. 09 (2013) P09001.
[65] S. T. Bramwell and P. C. W. Holdsworth, J. Condens. Matter Phys. **5**, L53 (1993).
[66] S. B. Khokhlachev, Zh. Exp. Teor. Fiz. **70**, 265 (1976) [Sov. Phys. JETP **43**, 137 (1976)], http://www.jetp.ac.ru/cgi-bin/e/index/e/43/1/p137?a=list.
[67] V. Irkhin and A. Katanin, Phys. Lett. A **232**, 143 (1997).
[68] T. Roscilde, V. Tognetti, R. Vaia, A. Cuccoli, and P. Verrucchi, Phys. Rev. B **67**, 18 (2003).
[69] S. K. Kim and S. B. Chung, SciPost Phys. **10**, 68 (2021).
[70] A. Cuccoli, T. Roscilde, R. Vaia, and P. Verrucchi, Phys. Rev. Lett. **90**, 167205 (2003).
[71] N. Rogado, Q. Huang, J. W. Lynn, A. P. Ramirez, D. Huse, and R. J. Cava, Phys. Rev. B **65**, 144443 (2002).
[72] M. Heinrich, H.-A. Krug von Nidda, A. Loidl, N. Rogado, and R. J. Cava, Phys. Rev. Lett. **91**, 137601 (2003).
[73] E. S. Klyushina, J. Reuther, L. Weber, A. T. M. N. Islam, J. S. Lord, B. Klemke, M. Månsson, S. Wessel, and B. Lake, arXiv:2012.02820.